

Autothermal Oxidative Coupling of Methane over Pt/Al₂O₃ Catalysts Doped with Rare Earth Oxides

Sven Schardt, Felix Ehrlich and Patrick Lott*

DOI: 10.1002/cite.202300165

This is an open access article under the terms of the [Creative Commons Attribution-NonCommercial](#) License, which permits use, distribution and reproduction in any medium, provided the original work is properly cited and is not used for commercial purposes.



Supporting Information
available online

The effect of rare earth oxides as dopants on the Pt-governed oxidative coupling of methane (Pt-OCM) is investigated. The addition of 20 wt.-% of La-, Nd-, Sm-, and Pr-oxides to the support benefits the C₂ product selectivity and offers the potential to enhance the catalyst stability. Compared to the reference catalyst Pt/Al₂O₃, the addition of Sm₂O₃ increased the total selectivity by up to 23 %. Furthermore, La₂O₃ addition was found beneficial with respect to the (thermal) stability of the catalyst. Dopant content variations uncovered that the catalyst formulation with 20 wt.-% La₂O₃ represents an optimum regarding performance and stability.

Keywords: Acetylene, Dopants, High-temperature catalysis, Oxidative coupling of methane, Rare earth oxides

Received: September 28, 2023; *revised:* April 23, 2024; *accepted:* April 24, 2024

1 Introduction

The simplest hydrocarbon, methane (CH₄), which nowadays originates not only from fossil natural gas [1], but also from fermentation of biomass [2] and power-to-gas processes using renewable energy [3], plays a key role in chemical industry. It is of great interest for a variety of different applications such as (bio-)methane pyrolysis [4–6], dry reforming [7, 8], or catalytic partial oxidation (CPOX) for syngas production [9, 10]. The main obstacle for any of these processes is the comparably strong C–H bond of the CH₄ molecule, necessitating either high energy input or suitable catalysts for C–H bond scission [11]. In the context of CPOX, mainly platinum group metals (PGMs) like Pt and Rh [10, 12] are applied for CH₄ activation, although also non-precious metals like Ni [13] or V [14] were shown to be active. Downstream process steps allow to convert the syngas into value-added products, e.g., production of olefins and aliphatic compounds via the Fischer-Tropsch-process [15]. However, a direct conversion of methane to value-added chemicals would have an even higher economical and also ecological appeal.

In contrast to many other methane conversion routes, oxidative coupling of methane (OCM) directly yields C₂ products, which are of great interest and need in the chemical industry [16, 17], thus making OCM an attractive route for CH₄ upgrading to higher-value products [17, 18]. In 1982, Keller and Bhasin [19] discovered OCM for C₂ species production and investigated several metal oxide catalysts supported on α -Al₂O₃. Since then, many different cata-

lysts [20–22] and operation conditions [23, 24] have been evaluated. One of the most frequently used systems in recent publications is Mn-Na₂WO₄/SiO₂ [25, 26], which predominantly yields ethane (C₂H₆) and ethylene (C₂H₄) with comparably high C₂ selectivity (>70 %) but only low methane conversion rates (<40 %) [26].

Notably, mechanistic studies by Lunsford [27] propose an interplay between both homogeneous and heterogeneous catalysis during OCM, with metal surface sites serving as active centers for methyl radical (CH₃•) generation and subsequent recombination of these radicals in the gas phase to form C₂H₆. In the context of the Mn-Na₂WO₄/SiO₂ catalyst, Zhou et al. [28] investigated several transition earth oxides for their CH₃• generation capability and showed that rare earth oxides (REOs), especially Sm₂O₃, can increase the C₂ selectivity by enhancing the formation of CH₃• radicals.

As demonstrated by Hohn et al. [29], the operation of Pt- and Rh-based catalysts at high space velocities and thus low residence times mainly yields acetylene (C₂H₂) instead of C₂H₆ and C₂H₄ at comparably high methane conversions well above 50 %. Due to high temperatures resulting from the simultaneously ongoing CPOX at very short contact

¹Sven Schardt <https://orcid.org/0000-0003-3615-3095>,

¹Felix Ehrlich, ¹Dr. Patrick Lott

<https://orcid.org/0000-0001-8683-2155> (patrick.lott@kit.edu)

¹Karlsruhe Institute of Technology (KIT), Institute for Chemical Technology and Polymer Chemistry, Engesserstr. 20, 76131 Karlsruhe, Germany.

times, the reaction runs autothermally and consequently an additional energy input becomes obsolete. Recent studies by Chawla et al. [30, 31] combining experiments and simulations underscore that methyl radicals play a key role during Pt-catalyzed OCM (Pt-OCM). These $\text{CH}_3\cdot$ species mainly originate from homogeneous gas phase chemistry that is enabled by the high reaction temperatures, and their formation typically involves the attack of an H radical, an OH radical, or an O radical on the CH_4 molecule. Overall, high CH_4 conversion, high C_2H_2 selectivity, additional syngas formation, and the possibility of establishing an autothermal process make Pt-OCM particularly attractive for potential industrial applications. However, for industrial viability the durability of the catalyst materials in demanding high-temperature reaction environments as well as the product selectivities need to be improved.

In this context, the present study aims at improving the C_2 product selectivities, in particular to the main C_2 product C_2H_2 , as well as the catalyst stability during Pt-OCM. For this, REOs that can contribute to methyl radical formation are added as dopants to Pt/ γ - Al_2O_3 -OCM-catalysts by preparing REO/ γ - Al_2O_3 support materials in different weight shares using La, Sm, Pr, and Nd as rare earth metals and subsequent impregnation with Pt. After washcoating of monolithic substrates, the resulting catalyst samples are tested for their activity and product selectivity in a kinetic test bench. An undoped Pt/ γ - Al_2O_3 -catalyst serves as reference.

2 Methodology and Experimental Setup

2.1 Sample Preparation

Depending on the desired amount of REO in the sample, two different methods were used for powder catalyst preparation. For REO contents < 40 wt.-%, incipient wetness impregnation (IWI) was applied. For this, the respective rare earth nitrate (REN) and the platinum precursor were dissolved together in an amount of deionized water equal to the pore volume of γ - Al_2O_3 (Puralox, Sasol; calcined for 5 h at 700°C) that served as a basis for the support. The different precursors used are given in Tab. S1 (Supporting Information). The resulting sample was dried at 80°C for at least 4 h and afterwards calcined for 5 h at 500°C , both in static air. Samples with an REO content ≥ 40 wt.-% were synthesized by coprecipitation (CP). For this, both REN and alumina nitrate were dissolved in deionized water in the desired weight ratio. Under continuous stirring, concentrated NaOH was slowly added to the solution until reaching a pH value of about 9. The resulting gel-like liquid obtained after additional 2.5 h of stirring was subsequently filtrated and washed with deionized water until the pH value of the filtrate was at about 7. After 4 h of drying at 80°C , the obtained solid was calcined for 5 h at 700°C in static air. After an IWI of the platinum precursor, the powder catalyst

was calcined for 5 h at 500°C in static air. As a reference, one sample with pure La_2O_3 as support was prepared analogously via IWI.

Subsequently, the samples were coated onto cordierite honeycomb monoliths (Corning, length $l =$ diameter $d = 10$ mm, 400 CPSI) according to the method described by Karinshak et al. [32]. After mixing the catalyst powder with deionized water and a binder ($\text{AlO}(\text{OH})$, boehmite, Disperal P2, Sasol) in a ball mill (Pulverisette 6, Fritsch) for 2×5 min at 300 rpm with 10 min pause between the two consecutive milling runs, the resulting slurry was carefully coated onto the monolith until an active metal loading of 30 g ft^{-3} was reached. The monolithic sample was subsequently calcined for 5 h at 550°C in static air. As the Pt-loading is 1 wt.-% for all samples, the nomenclature of the final catalyst used hereinafter refers only to the dopant content, e.g., 20Sm refers to 1 wt.-% Pt/20 wt.-% $\text{Sm}_2\text{O}_3/\text{Al}_2\text{O}_3$ and 100Al refers to 1 wt.-% Pt/ Al_2O_3 .

2.2 Catalytic Activity Test

Activity tests were conducted in a test-bench that was already described in detail in a previous publication [30]. The diluent N_2 was premixed with CH_4 and O_2 and preheated to 190°C before entering the reactor located in a furnace. The reactor itself consists of quartz glass and has an inner diameter of 20 mm but is reduced to 10 mm at the reaction zone, where the monolithic catalyst is located. The furnace was heated to 500°C during the duration of an experiment. For beneficial heat transfer, an uncoated monolith (heat shield) was placed 10 mm upstream of the catalyst. A type-S thermocouple 5 mm downstream of the catalyst monitors the temperature inside the reactor. The effluent gas was cooled to 190°C , diluted with additional N_2 behind the reactor (improves the signal-to-noise ratio in the analyzer) and analyzed in an online Fourier-transform infrared spectrometer (FTIR, MultiGas 2030, MKS Instruments).

A paramagnetic oxygen detector (Magnos28, ABB GmbH) monitored the oxygen consumption during the reaction and an NO dosage unit behind the reactor allowed to introduce NO as a tracer gas to account for volume changes of the gas stream due to the reactions taking place. Based on the carbon and oxygen balances we generously estimated the error regarding the cumulated C-containing species as $\pm 7\%$ and the error regarding the cumulated O-containing species as $\pm 20\%$ in the worst case. The error from misdosing of the mass flow controllers (MFCs, Bronkhorst) that were used for feeding CH_4 , O_2 , and N_2 , was considered low, as the MFC calibrations were confirmed on a regular basis. In contrast, disadvantageous signal-to-noise ratios for the gas species in the FTIR analyzer were considered most relevant; the fluctuations of CO_2 concentration data were particularly pronounced. Since the paramagnetic oxygen detector provides reliable online data only in the percentage range, the uncertainty regarding O_2

concentration increases with rising oxygen consumption and contributes substantially to the error in the O-balance.

While the N₂ content was varied in order to find the most advantageous reaction conditions, all experiments were run at a GHSV of 458 000 h⁻¹ and a C:O ratio of 0.55. These values were found as optimum during a broad parameter study to be published soon. Once starting the experiment at 80 vol.-% N₂ in feed, the reaction ignites and runs autothermally.

2.3 Characterization of the Catalyst

Elemental analysis of the sample composition, namely, Pt- and dopant content, was done by inductively coupled plasma optical emission spectroscopy (ICP-OES) in an iCAP 7600 DUO analyzer (Thermo Fisher Scientific). X-ray diffraction (XRD) patterns provide structural information and were obtained in a Bruker D8 Advance diffractometer using Cu-K α radiation with a wavelength of 1.54 Å and scanning from 20° to 80° in 0.016° steps, and in a PANalytical X'Pert Pro diffractometer using Cu-K α radiation with a wavelength of 1.54 Å and scanning in a range from 20° to 80° with a step size of 0.017° and a step time of 1 s.

N₂ physisorption was conducted in a BELSORP-mini II (BEL Japan, Inc.) to analyze surface properties of the powder catalysts, which were pretreated by degassing at 300 °C for 2 h. The surface area was determined by the Brunauer-Emmett-Teller (BET) method [33] based on the adsorption-desorption curves. Analogous to previous studies [34–36], CO chemisorption measurements were carried out in a continuous flow reactor operated at atmospheric pressure and equipped with an infrared analyzer (X-Stream Enhanced XEGK compact gas analyzer, Emerson Electric Co.) that monitors the CO and CO₂ content of the reaction gas. After placing the quartz glass tubular reactor loaded with the catalyst inside a furnace, the catalyst was oxidized at 500 °C for 20 min in air, cooled to 400 °C in N₂, and subsequently reduced with 4 vol.-% H₂ in N₂ for 60 min. After the reductive period the reactor was cooled down to 25 °C in N₂ and exposed to 1 vol.-% CO in N₂ for 60 min to ensure coverage of all active sites by CO. After flushing (60 min) to remove gas phase CO, a temperature-programmed desorption (TPD) of pre-adsorbed CO yielded the noble metal dispersion under the assumption of a CO:Pt adsorption stoichiometry of 1:1 [37].

3 Results and Discussion

3.1 Variation of the REO Dopant

In order to evaluate the impact of different REO dopants on the OCM activity of Pt/Al₂O₃-based catalysts, samples doped with La₂O₃, Sm₂O₃, Nd₂O₃, and Pr₆O₁₁ were subject to kinetic testing. For the sake of comparability, the REO loading of 20 wt.-% was kept constant for all sam-

ples. The results of the kinetic tests are summarized in Fig. 1 (CH₄ conversion, C₂ species selectivity), Fig. 2 (CO and H₂O selectivity, temperature), and Fig. S1 in the Supporting Information (CO₂ selectivity). Fig. 1A shows the total C₂ selectivity of the REO-doped samples as well as of Pt/Al₂O₃ that serves as a REO-free reference sample. Irrespective of the catalyst formulation, the C₂ selectivity rises with decreasing N₂ dilution until reaching a maximum that is found at 50 vol.-% N₂ for almost all samples. Therefore, catalyst operation conditions with 50 vol.-% N₂ in the feed will serve as reference point throughout this study. 20Pr is the only sample that behaves differently and which has its maximum at 45 vol.-%. Among the samples tested herein, the Sm-doped catalyst (20Sm) achieves the highest C₂ selectivity of 11.2 %, followed by 20Nd with 10.8 % and 20La with 10.3 %.

Figs. 1B–D illustrate the selectivity of each individual C₂ product. C₂H₆ selectivities (Fig. 1B) are generally very low (<1 %) and decline to almost zero for dilutions lower than 55 %. Only two data points exceed 1 %, namely, 20Nd at 55 vol.-% dilution with 1.01 % and 20Pr at 50 vol.-% dilution with 1.22 %. Irrespective of the catalyst formulation, the formation of C₂H₄ (Fig. 1C) starts at 75 % dilution and remains at about 2 % during the N₂ content variation. In analogy to the trends observed for S(C₂H₆), 20Nd and 20Pr reach S(C₂H₄) maxima of 4.8 % at 55 vol.-% dilution and 5.6 % at 50 vol.-%, respectively. Notably, 20Pr and 20Nd show deviances also for S(C₂H₂) (Fig. 1D) under these operation conditions, as the selectivities drop at 50 vol.-% and 55 vol.-% N₂ dilution, respectively. Except for these two datapoints, the stepwise decrease of the N₂ dilution results in a selectivity towards C₂H₂ that clearly exceeds the selectivity towards C₂H₄ and C₂H₆ for all catalysts tested. The highest S(C₂H₂) of 8.5 % is found for 20La at 50 vol.-% dilution.

To set the product selectivities in relation, Fig. 1E shows the corresponding methane conversion for the different catalyst samples. Except for 20Pr at 50 vol.-% dilution (X(CH₄) = 77 %), all catalysts convert more than 80 % of CH₄ under all conditions applied. In general, CH₄ conversion rises with decreasing N₂ dilution, drops at moderate N₂ dilutions reaching a local minimum at 55 vol.-% and rises again if the dilution is further decreased (Fig. 1E). Note that methane conversions between 87 % and 92 % are found for the operation conditions that result in maximum C₂ selectivity. However, the maximum C₂ selectivity does not necessarily correspond to the highest CH₄ conversion observed. Although we assume that uncertainties due to noisy raw data (see Sect. 2.2) may contribute to this observation, also chemical effects as well as the temperature in the reactor play a key role as discussed below in more detail.

In contrast to the C₂ selectivity, the catalyst formulation has an only minor impact on the CO selectivity and the trends during the dilution variation are very similar (Fig. 2A), whereas those for H₂O vary strongly (Fig. 2B). In particular, at the highest dilution of 80 vol.-% of N₂ in the feed there is a difference of approx. 10 % in CO selectivity

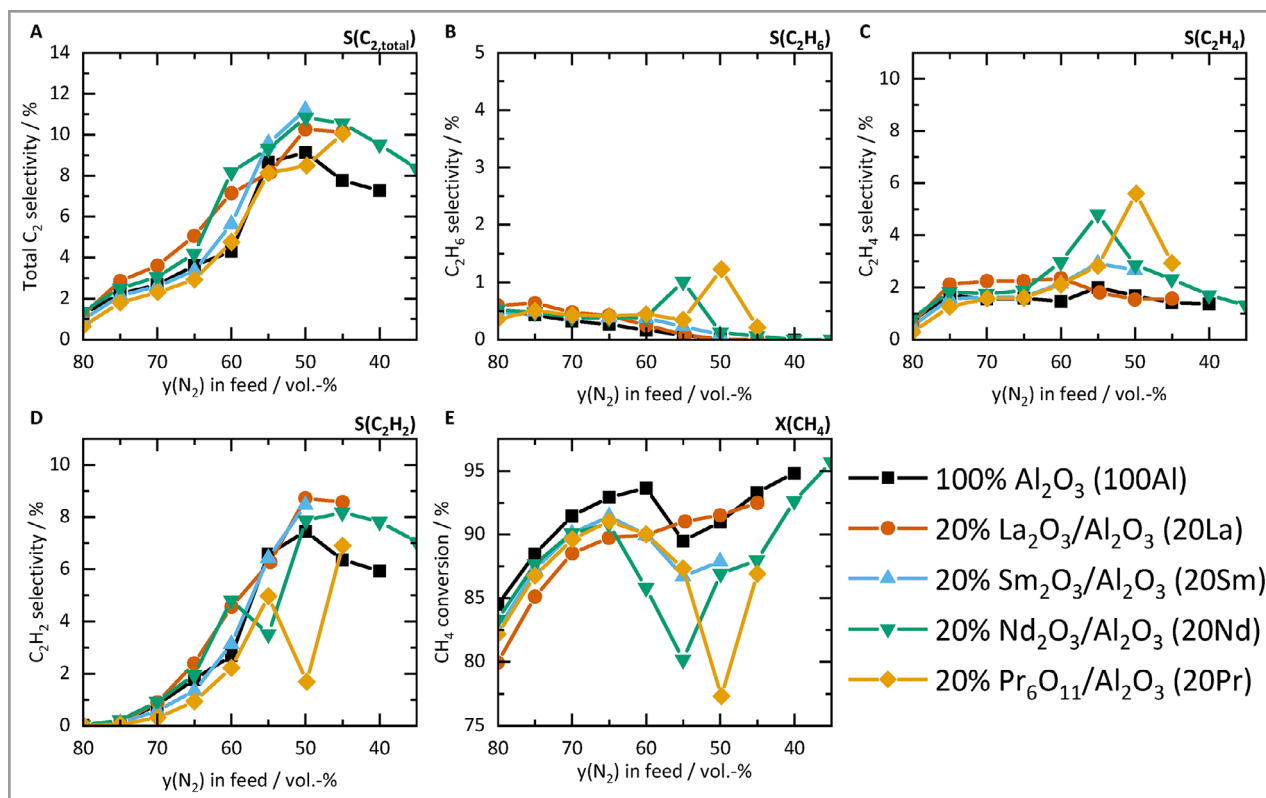


Figure 1. Various product parameters as (A) total C₂ selectivity, (B) CH₄ conversion, (C) C₂H₂, (D) C₂H₄, and (E) C₂H₆ selectivity versus N₂ content in feed at a GSHV of 458 000 h⁻¹ and a C:O ratio of 0.55 for the investigated catalysts.

between the undoped 100Al sample that exhibits the highest CO selectivity of 68.4 % and 20Pr with the lowest CO selectivity of 59.8 %. Aside from the fact that the shape of the selectivity curve is identical, the difference between the highest and the lowest value reduces to only 1 % at 50 vol.-% N₂ dilution. The continuous decrease in CO selectivity if the dilution is decreased from 60 vol.-% onwards might then be the result of the temperature increase in the reactor (Fig. 2C)

that promotes the OCM reaction and therefore C₂ species formation rather than the CPOX reaction resulting in CO formation.

As underscored by the data in Fig. 1A, C₂ formation is promoted indeed and particularly the formation of C₂H₂, which is the most stable C₂ product at these temperatures [38], increases (Fig. 1B). Moreover, REO-containing samples tend to yield higher water levels than the reference catalyst

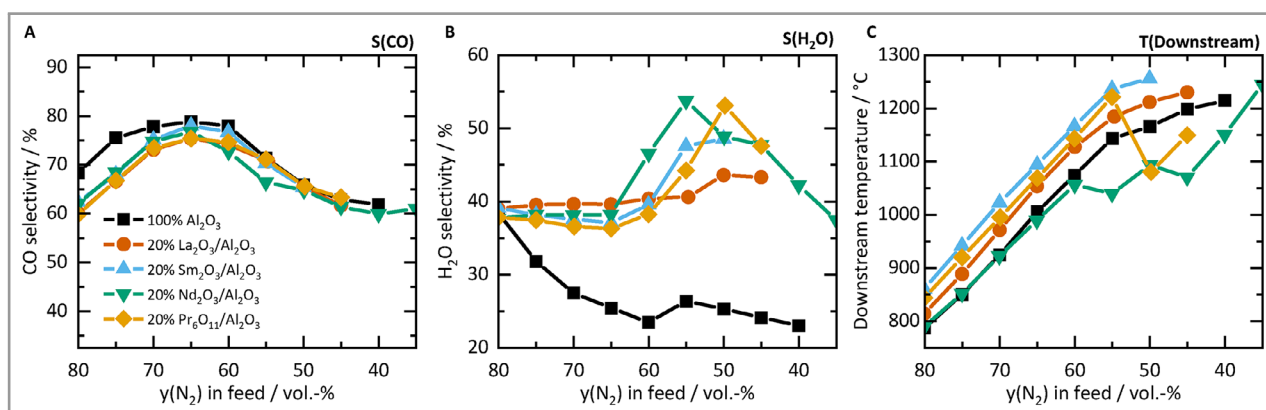


Figure 2. (A) CO selectivity, (B) H₂O selectivity, and (C) downstream temperature versus N₂ content in feed at a GSHV of 458 000 h⁻¹ and a C:O ratio of 0.55 for the investigated catalysts.

100Al (Fig. 2B); the most pronounced difference is found at 50 vol.-% dilution, namely, $S(\text{H}_2\text{O})$ of 25.3 % for 100Al versus 53.1 % for 20Pr. Presumably, the higher water levels are a consequence of the REO-promoted dehydrogenation of ethane that is formed as intermediate product during OCM [39, 40], and subsequent oxidation of the evolving H_2 . Last but not least, CO_2 is formed as a byproduct (Fig. S1). Despite the rather pronounced fluctuations of the CO_2 concentration data obtained from the FTIR analyzer, the selectivity trends clearly suggest that CO_2 formation declines with decreasing dilution, which directly corresponds to the rising C_2 species levels (Fig. 1A) enabled by the rising temperature in the reactor (Fig. 2C).

The majority of the doped samples show an approximately 100 °C higher downstream reaction temperature compared to 100Al (Fig. 2C). Since sufficiently high temperatures were reported as prerequisite for methyl radical formation, subsequent gas phase recombination to form C_2H_6 , and subsequent dehydrogenation [27, 29–31], this more pronounced heat evolution is, in addition to methyl radical production from heterogeneous reaction pathways, an important factor that enables the higher C_2 selectivities observed over the REO-doped catalyst samples (Fig. 1A). In this context, the temperature trends of 20Nd and 20Pr stand out in the data shown in Fig. 2C. They exhibit a pronounced drop at 55 vol.-% and 50 vol.-% dilution, respectively, which directly corresponds to the C_2 product species composition obtained (Figs. 1B–D). The correlation between temperature and product species is most pronounced for the formation of acetylene (Fig. 1B), which is the most stable of the three C_2 species at high temperatures [38]. Moreover, the CH_4 conversion drop observed for almost all samples (Fig. 1E) is also related to the increasing temperature (Fig. 2C). This conversion drop is most significant for 20Pr and 20Nd, for which simultaneously a $S(\text{C}_2\text{H}_2)$ drop and both a $S(\text{C}_2\text{H}_4)$ and $S(\text{C}_2\text{H}_6)$ rise occur, which is not observed for any other sample. On the other hand, 20La is the only catalyst that shows a continuous trend in methane conversion over the dilution variation.

The correlation between the temperature, the conversion of oxygen, and the product composition became particularly clear in recent mechanistic studies by Chawla et al. [30, 31]. On the one hand, oxidation reactions typically consume the majority of O_2 , which results in pronounced heat evolution. OH or O radicals, which form under these harsh conditions, attack CH_4 and result in methyl radical formation. However, despite the high oxygen content in the feed gas stream, also pyrolytic reaction pathways become relevant, during which H radicals attack CH_4 molecules to form species [31]. Herewith, the OCM reaction mechanism exhibits parallels to reactions taking place during non-oxidative coupling of methane (NOCM) [18, 41, 42]. Since oxygen was essentially fully converted under most of the conditions applied in this study, it is assumed that both oxidative and pyrolytic pathways are relevant over the REO-doped catalyst samples investigated herein.

In summary, REO addition to a Pt/ Al_2O_3 OCM catalyst was found to be beneficial, as the C_2 selectivity was at least equal to the reference sample 100Al at high dilutions and promoted at lower dilutions. As for both Pt-OCM [30] and REO-driven OCM [28] a dependency on gas phase reactions and thus methyl radical formation was reported previously, one can deduce that for our catalyst systems these effects occur simultaneously, hereby improving C_2 formation. Zhou et al. [28] found Sm_2O_3 as the most effective compound for $\text{CH}_3\cdot$ generation, which outperformed other REOs by far; however, the same study also revealed La_2O_3 as the dopant yielding the highest C_2 selectivity, followed by Sm_2O_3 . In our study on Pt-OCM, Sm and Nd were found as most suitable dopants enabling the highest total C_2 selectivity, and La-doping was found to be almost equally beneficial. More importantly, 20La showed the highest selectivity towards acetylene and in contrast to the other samples lacks the conversion drop around 55 vol.-% N_2 .

The predominant support compound Al_2O_3 undergoes a phase change from its γ -phase towards the α -phase at temperatures >1200 °C [43], which are present during Pt-OCM. Please note that the temperature shown in Fig. 2C is the downstream temperature monitored with a distance of about 5 mm from the catalyst and is therefore not representing the temperature inside the catalyst itself, which is likely even higher [29–31]. La_2O_3 is known to stabilize Al_2O_3 by either inhibiting a phase transition or by forming mixed oxides [44–46]. The high-temperature stability of 20La is most likely related to the ability to delay phase changes of metal oxide supports at high temperatures, which makes La a frequently used dopant for Al_2O_3 [47–49]. This leads to a more stable catalytic system exhibiting a steadier performance without significant drops in activity and selectivity.

Nevertheless, the comparison of XRD data of the fresh (Fig. 3A) and the spent catalysts (Fig. 3B) suggests that like for any other sample a phase change towards α - Al_2O_3 occurred also for the La-containing catalyst. Although the data quality impedes quantitative conclusions, one can assume that exposure of the REO-doped samples to OCM conditions does not initiate major transformations of the 20 wt.-% REO content, as no rare earth compounds are visible in the XRD patterns of the spent samples. However, all samples show the characteristic reflexes of α - Al_2O_3 . Especially for 20La this means that despite the lanthanum is aiding the performance and stability of the catalyst, it cannot prevent the phase change of alumina. More likely it supports the washcoat micro- and macrostructure, possibly via the formation of stable mixed oxides, which may maintain conversion and selectivity throughout the phase change.

Wang et al. [20] investigated the activity of La_2O_3 for OCM and claim that the lattice oxygen of the lanthanum oxide significantly contributes to the methyl radical formation. According to the authors, the C–H bond cleavage is promoted by the different Lewis acidic and Brønsted basic lattice sites (La^{3+} and O^{2-} , respectively), resulting in an

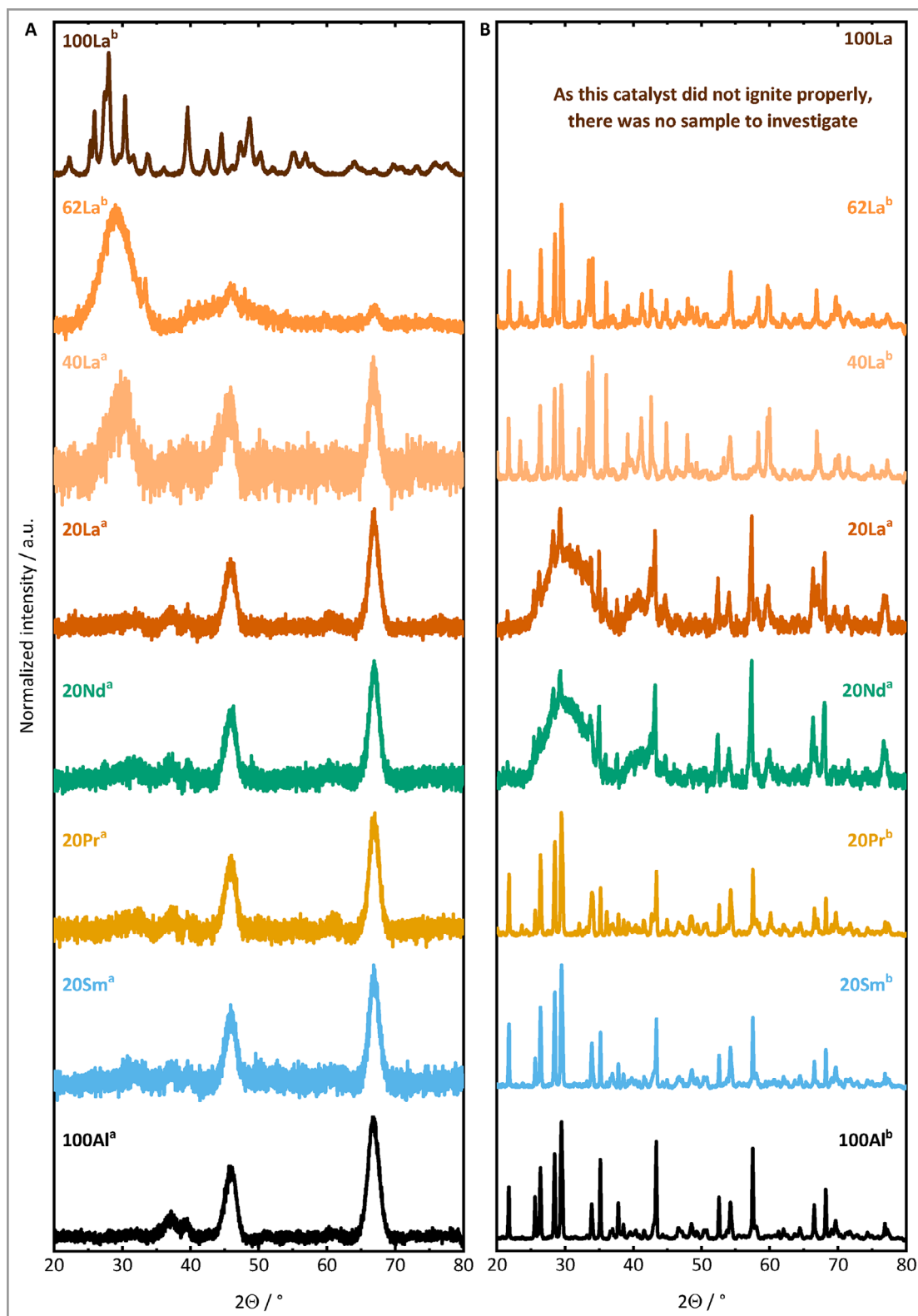


Figure 3. X-ray diffractograms of the fresh (A) and used (B) catalysts. Samples with ^a were recorded with the Bruker XRD, samples with ^b with the PANalytical XRD. Please note the disadvantageous signal-to-noise ratio due to the low sample mass for the used samples.

interplay with the present oxygen and $\text{CH}_3\cdot$ species. The same effects may be relevant also for the catalyst used herein.

Siakavelas et al. [22] examined the addition of La and Sm to a Li/Ce-based OCM catalyst. For their system, the REOs increased both the CH_4 conversion and the total C_2 yield, but their catalysts solely yielded C_2H_4 and C_2H_6 . Although REO doping of our Pt-based catalyst system slightly decreased the CH_4 conversion (Fig. 1E), the total C_2 selectivity was clearly promoted, in particular C_2H_2 formation, which is attributed to the higher methyl radical formation capability of the doped catalyst formulation [28].

In addition to their contribution to the formation of intermediate species like $\text{CH}_3\cdot$, the REO doping also impacts the noble metal particles. Tankov et al. [50] investigated a Pt-Pr-Al-based catalyst for the dry reforming of methane and found a positive influence of the REO on the catalytic activity. They claim that praseodymium oxide increases the Pt dispersion and facilitates oxidation state changes to metallic Pt species, which are considered more active for methane activation than platinum oxide particles. Since Pt^0 was postulated to be the active site for methane conversion during both CPOX and dry reforming [51, 52], one can assume analogously that a metallic character of our noble metal particles induced by the REO addition contributes to the high Pt-OCM activity. Furthermore, an impact of the dopants on the noble metal dispersion based on our CO chemisorption measurements can be assumed. Unfortunately, REOs impede precise and quantitative CO chemisorption experiments [53], as also underscored by our characterization data (Tab. S2).

Our CO chemisorption data suggest Pt dispersions well above 100 % for REO-containing samples, which are attributed to a spillover of CO from the noble metal to the support, in particular the REO sites. If the dispersion is calculated under consideration of a possible adsorption of CO also on rare earth metal surface sites, the dispersion values drop below 10 %, which seems unrealistically low when the 100Al sample (Pt dispersion of 64 %, Tab. S2) is considered as reference. Although these data do not allow a quantitative statement, one can assume that REO addition results in alteration of the noble metal particle sizes, which may also be a consequence of the change in specific surface area. Although surface area and pore volume are expected to play an only minor role regarding the activity of the doped samples, a lower surface area of heterogeneous catalysts frequently benefits larger noble metal particles and thus governs the catalyst performance indirectly.

All REO-containing samples exhibit a surface area of about $90 \text{ m}^2\text{g}^{-1}$ and a pore volume of about $0.29 \text{ cm}^3\text{g}^{-1}$ (Tab. S3). Compared to the reference sample 100Al with a specific surface area $A_{\text{BET}} = 141.3 \text{ m}^2\text{g}^{-1}$ and a pore volume $V_p = 0.42 \text{ cm}^3\text{g}^{-1}$ (Tab. S3), REO doping reduces the surface area. Nevertheless, the doped catalysts outperform 100Al especially at high temperatures in terms of $S(\text{C}_2)$, which is most likely related to the REO-promoted $\text{CH}_3\cdot$ forma-

tion. Ultimately, elemental analysis uncovered only marginal variations in the actual Pt loading and confirmed the REO loading (Tab. S4), hence no significant impact on the catalyst performance is expected.

3.2 Influence of the La_2O_3 Content on the Catalytic Activity

As lanthanum oxide exhibited a particularly positive effect by stabilizing the catalyst along with an increased selectivity towards C_2 species, the lanthanum content in the system was varied. To determine the optimal amount of La_2O_3 , the dopant content was varied and the impact on OCM was determined by means of kinetic measurements. Fig. 4 shows the dependency of the different C_2 product selectivities on the lanthanum content in the catalyst. As operation conditions 50 vol.-% N_2 in the feed, a C:O ratio of 0.55, and a space velocity of $458\,000 \text{ h}^{-1}$ were chosen, since the 20La catalyst exhibited its performance maximum under these conditions (Fig. 1). The reaction over the entirely Al_2O_3 -free sample 100La did not ignite properly during exposure to the reactive atmosphere and could not maintain the OCM reaction under the parameters chosen, whereas all other samples produced C_2 species.

As depicted in Fig. 4A, the production of C_2H_6 is negligible for all catalyst formulations tested. Selectivities to C_2H_4 are similar for all samples, ranging from 1.5 % for 20La to 2.0 % for 62La, and C_2H_2 is the main C_2 product, irrespective of the catalyst formulation. While the La-free reference sample as well as the samples with 40 wt.-% and 62 wt.-% show similar selectivity towards acetylene (7.5 %, 7.8 %, and 7.8%, respectively), 20La exhibits the highest C_2H_2 selectivity (8.7%) and the highest total C_2 selectivity (10.3 %) of all samples. Ultimately, the downstream temperature depicted in Fig. 4B varies between approx. $1163 \text{ }^\circ\text{C}$ (62La) and $1218 \text{ }^\circ\text{C}$ (40La); notably catalysts that achieve higher temperatures do not necessarily correspond to higher total C_2 selectivity, although high temperatures are vital for methyl radical formation in the gas phase [31].

As already discussed in the previous section, alumina seems to play a crucial role in Pt-OCM and appears to be necessary to run the autothermal Pt-OCM reaction because the reaction did not ignite properly over 100La. Although there are several studies on OCM that report relevant C_2 species production on pure La_2O_3 which served either as catalyst or as support material [20, 39, 54], these studies activate and sustain the OCM reaction via external heat. In contrast, during our Pt-OCM the activation energy needed for ignition of the reaction was provided solely by exothermic oxidation reactions, which allows for autothermal operation [30]. Similar to our study, Sarsani et al. [55] ran OCM under autothermal conditions, however, under different reaction conditions, namely, a C:O ratio of 2 (versus 0.55 in our study) and with a La-Ce-based catalyst. In conclusion, using only La_2O_3 as support seems not suitable

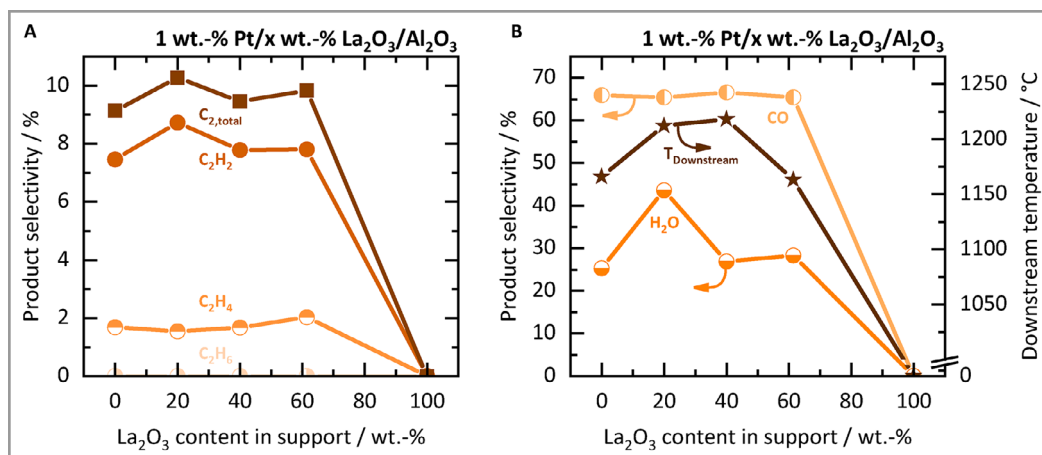


Figure 4. Selectivity towards (A) the three different C₂ species and (B) towards CO and H₂O and the downstream temperature measured 5 mm behind the catalyst versus the La₂O₃ content in the used support at 50 vol. % N₂ content in the feed, a GHSV of 458 000 h⁻¹, and a C:O ratio of 0.55.

for Pt-OCM under the conditions subject to our present study.

Since the temperature changes are only moderate when varying the La₂O₃ content ($\Delta T_{\max} = 55$ K), the differences in the performance regarding C₂ formation (Fig. 4A) are attributed to the REO content in the support. These findings are in analogy to results by Tankov et al. [50], who found an optimal amount of REO content for a Pt-Pr-Al catalyst system that was used for activating the CH₄ molecule during methane dry reforming.

With regard to structural parameters, the addition of increasing amounts of La₂O₃ to the Al₂O₃ support leads to a decreasing surface area (91 m²g⁻¹ for 20La versus 48 m²g⁻¹ for 62La; see Tab. S4). However, considering the product species trends shown in Fig. 4, the surface area seems to be a factor of minor importance in the context of OCM over Pt/La₂O₃-Al₂O₃ catalysts. Furthermore, the XRD patterns of the fresh as-prepared catalysts (Fig. 3A) show reflexes which are characteristic for La₂O₃ and that increase with the La-loading. Despite a poorer signal-to-noise ratio, these reflexes persist and do not seem to change also after using the samples under OCM conditions (Fig. 3B); hence, La₂O₃ does not undergo phase changes, which is in line with the studies on high-temperature stability of La-containing materials [44–46] as discussed already in the previous section in more detail.

4 Conclusion

To improve both activity and selectivity of Pt/Al₂O₃-based OCM catalysts, the influence of rare earth oxides (REOs) on the Pt-catalyzed oxidative coupling of methane (Pt-OCM) was investigated by means of kinetic testing. For this, Al₂O₃ was doped with various rare earth metal oxides (La₂O₃, Nd₂O₃, Pr₂O₃, Sm₂O₃) with a loading of 20 wt.-%. In a sec-

ond step, the La₂O₃ content was varied in order to determine the optimal dopant amount.

Regarding the total C₂ selectivity, the REO-doped samples outperformed the Pt/Al₂O₃ reference sample under most of the reaction conditions subject to this study. At 50 vol.-% N₂ in the feed, the Pt/Al₂O₃ catalyst achieved a total C₂ selectivity of 9.1 %, whereas the addition of 20 wt.-% Sm₂O₃ increased the total C₂ selectivity to 11.2 %, corresponding to an improvement of 23 %. Based on findings from previous studies [27, 28, 30, 31] the beneficial effect of REO addition was attributed to an enhanced methyl radical formation. The gas phase recombination of these radicals to form ethane and subsequent dehydrogenation steps ultimately led to the desired product acetylene. Furthermore, a pronounced water formation was observed during the kinetic tests upon introduction of REO dopants, which could be due to the oxidation of hydrogen that evolves during dehydrogenation from ethane and ethylene. The exothermicity of the hydrogen oxidation reaction would also explain the higher reaction temperature that promotes homogeneous reactions and benefits the formation of C₂H₂ that is the thermodynamically most favored C₂ species at temperatures well above 1000 °C as relevant in this study.

As determined by means of X-ray diffraction and kinetic testing, samples doped with La₂O₃ exhibit the highest stability with regard to catalyst structure and performance. Hence, the La-content was varied in order to evaluate whether higher REO loadings may promote OCM even more. 20 wt.-% La₂O₃/Al₂O₃ was determined as the most suitable support for Pt-OCM, as it yielded way higher C₂H₂ selectivities than the other samples in the content variation. Despite the positive influence of La₂O₃, a La₂O₃-only support was found to be insufficient for Pt-OCM as the reaction did not ignite properly and could not be maintained. This points to a key role of the Pt-Al interface for the OCM reaction, or more specifically for the underlying catalytic partial

oxidation of methane (CPOX) that provides the heat for the autothermal reactor operation during OCM.

In summary, the present study can serve as basis for further research on Pt-catalyzed OCM over novel catalyst materials. Future operando studies should investigate morphological changes of the support material as well as the actual impact of the REO on the Pt-OCM mechanism in more detail, as this will help to derive structure-activity correlations for the heterogeneous catalyst on the one hand and will provide valuable details on the reactions that take place on the catalyst surface and in the gas phase on the other hand. Ultimately, supplementing the present findings with such detailed knowledge can enable the design of industrially viable catalysts that exhibit high C₂ selectivity and high thermal stability.

Supporting Information

Supporting Information for this article can be found under DOI: <https://doi.org/10.1002/cite.202300165>. This section includes references already mentioned in primary literature relevant for this research [33].

Acknowledgment

The authors gratefully acknowledge O. Deutschmann for fruitful discussions and support regarding infrastructure, S. Bastian for technical support regarding the experimental setup, M. Makowiak and A. Deutsch for N₂ physisorption measurements, S. Struzek and A. de Giacinto for XRD measurements, C. Brown for his assistance with CO chemisorption measurements (all ITCP, KIT), and T. Bergfeldt (IAM-AWP, KIT) for elemental analysis via ICP-OES.

Open access funding enabled and organized by Projekt DEAL.

Symbols used

ΔT	[K]	temperature difference
$S(X)$	[-]	selectivity towards X

Sub- and Superscripts

max	maximum
-----	---------

Abbreviations

CP	coprecipitation
CPOX	catalytic partial oxidation (of methane)
FTIR	Fourier-transform infrared spectrometer

ICP-OES	inductively coupled plasma-optical emission spectroscopy
IWI	incipient wetness impregnation
NOCM	non-oxidative coupling of methane
OCM	oxidative coupling of methane
Pt-OCM	Pt-catalyzed oxidative coupling of methane
REN	rare earth nitrate
REO	rare earth oxide
TPD	temperature-programmed desorption
XRD	X-ray diffraction

References

- [1] C. Karakaya, R. J. Kee, *Prog. Energy Combust. Sci.* **2016**, *55*, 60–97. DOI: <https://doi.org/10.1016/j.pecs.2016.04.003>
- [2] P. Weiland, *Appl. Microbiol. Biotechnol.* **2010**, *85* (4), 849–860. DOI: <https://doi.org/10.1007/s00253-009-2246-7>
- [3] K. Ghaib, F.-Z. Ben-Fares, *Renewable Sustainable Energy Rev.* **2018**, *81*, 433–446. DOI: <https://doi.org/10.1016/j.rser.2017.08.004>
- [4] P. Lott, M. B. Mokashi, H. Müller, D. J. Heitlinger, S. Lichtenberg, A. B. Shirsath, C. Janzer, S. Tischer, L. Maier, O. Deutschmann, *ChemSusChem* **2023**, *16* (6), e202201720. DOI: <https://doi.org/10.1002/cssc.202201720>
- [5] N. Sánchez-Bastardo, R. Schlögl, H. Ruland, *Ind. Eng. Chem. Res.* **2021**, *60* (32), 11855–11881. DOI: <https://doi.org/10.1021/acs.iecr.1c01679>
- [6] A. Çelik, I. Ben Othman, H. Müller, P. Lott, O. Deutschmann, *React. Chem. Eng.* **2023**, *9* (1), 108–118. DOI: <https://doi.org/10.1039/D3RE00360D>
- [7] S. D. Angeli, S. Goßler, S. Lichtenberg, G. Kass, A. K. Agrawal, M. Valerius, K. P. Kinzel, O. Deutschmann, *Angew. Chem., Int. Ed.* **2021**, *60* (21), 11852–11857. DOI: <https://doi.org/10.1002/anie.202100577>
- [8] J. Titus, T. Roussi re, G. Wasserschaff, S. Schunk, A. Milanov, E. Schwab, G. Wagner, O. Oeckler, R. Gl aser, *Catal. Today* **2016**, *270*, 68–75. DOI: <https://doi.org/10.1016/j.cattod.2015.09.027>
- [9] O. Deutschmann, L. D. Schmidt, *AIChE J.* **1998**, *44* (11), 2465–2477. DOI: <https://doi.org/10.1002/aic.690441114>
- [10] A. Bitsch-Larsen, R. Horn, L. D. Schmidt, *Appl. Catal., A* **2008**, *348* (2), 165–172. DOI: <https://doi.org/10.1016/j.apcata.2008.06.036>
- [11] R. Horn, R. Schl gl, *Catal. Lett.* **2015**, *145* (1), 23–39. DOI: <https://doi.org/10.1007/s10562-014-1417-z>
- [12] M. C. Huff, P. M. Torniaainen, L. D. Schmidt, *Catal. Today* **1994**, *21* (1), 113–128. DOI: [https://doi.org/10.1016/0920-5861\(94\)80038-3](https://doi.org/10.1016/0920-5861(94)80038-3)
- [13] L. D. Vella, S. Specchia, *Catal. Today* **2011**, *176* (1), 340–346. DOI: <https://doi.org/10.1016/j.cattod.2010.11.068>
- [14] M. M. Koranne, J. G. Goodwin, G. Marcelin, *J. Catal.* **1994**, *148* (1), 378–387. DOI: <https://doi.org/10.1006/jcat.1994.1218>
- [15] A. Aguirre, E. Scholman, J. van der Shaaf, M. F. Neira d'Angelo, *Chem. Eng. J.* **2021**, *409*, 128139. DOI: <https://doi.org/10.1016/j.cej.2020.128139>
- [16] J. S. Valente, R. Quintana-Sol rzano, H. Armend riz-Herrera, J.-M. M. Millet, *ACS Catal.* **2023**, 1693–1716. DOI: <https://doi.org/10.1021/acscatal.2c05161>
- [17] P. Lott, O. Deutschmann, *Proc. Combust. Inst.* **2023**, *39* (3), 3183–3215. DOI: <https://doi.org/10.1016/j.proci.2022.06.001>
- [18] P. Schwach, X. Pan, X. Bao, *Chem. Rev.* **2017**, *117* (13), 8497–8520. DOI: <https://doi.org/10.1021/acs.chemrev.6b00715>

- [19] G. E. Keller, M. M. Bhasin, *J. Catal.* **1982**, *73* (1), 9–19. DOI: [https://doi.org/10.1016/0021-9517\(82\)90075-6](https://doi.org/10.1016/0021-9517(82)90075-6)
- [20] S. Wang, S. Li, D. A. Dixon, *Catal. Sci. Technol.* **2020**, *10* (8), 2602–2614. DOI: <https://doi.org/10.1039/D0CY00141D>
- [21] A. L. Tonkovich, R. W. Carr, R. Aris, *Science* **1993**, *262* (5131), 221–223. DOI: <https://doi.org/10.1126/science.262.5131.221>
- [22] G. I. Siakavelas, N. D. Charisiou, A. Alkhoori, V. Sebastian, S. J. Hinder, M. A. Baker, I. V. Yentekakis, K. Polychronopoulou, M. A. Goula, *J. Environ. Chem. Eng.* **2022**, *10* (2), 107259. DOI: <https://doi.org/10.1016/j.jece.2022.107259>
- [23] B. Michorczyk, J. Sikora, B. Kordon-Łapczyńska, D. Gawel, I. Czekaj, *Catalysts* **2022**, *12* (1), 54. DOI: <https://doi.org/10.3390/catal12010054>
- [24] A. S. Bodke, S. S. Bharadwaj, L. D. Schmidt, *J. Catal.* **1998**, *179* (1), 138–149. DOI: <https://doi.org/10.1006/jcat.1998.2224>
- [25] S. Arndt, T. Otremba, U. Simon, M. Yildiz, H. Schubert, R. Schomäcker, *Appl. Catal., A* **2012**, *425–426*, 53–61. DOI: <https://doi.org/10.1016/j.apcata.2012.02.046>
- [26] M. Kim, S. Arndt, M. Yildiz, R. Schomäcker, O. Görke, J.-U. Repke, G. Wozny, H. R. Godini, *Chem. Eng. Res. Des.* **2021**, *172*, 84–98. DOI: <https://doi.org/10.1016/j.cherd.2021.04.029>
- [27] J. H. Lunsford, *Angew. Chem., Int. Ed.* **1995**, *34* (9), 970–980. DOI: <https://doi.org/10.1002/anie.199509701>
- [28] Q. Zhou, Z.-Q. Wang, Z. Li, J. Wang, M. Xu, S. Zou, J. Yang, Y. Pan, X.-Q. Gong, L. Xiao, J. Fan, *ACS Catal.* **2021**, *11* (23), 14651–14659. DOI: <https://doi.org/10.1021/acscatal.1c03496>
- [29] K. L. Hohn, P. M. Witt, M. B. Davis, L. D. Schmidt, *Catal. Lett.* **1998**, *54* (3), 113–118. DOI: <https://doi.org/10.1023/A:1019092308769>
- [30] J. Chawla, S. Schardt, S. D. Angeli, P. Lott, S. Tischer, L. Maier, O. Deutschmann, *Catalysts* **2022**, *12* (2), 189. DOI: <https://doi.org/10.3390/catal12020189>
- [31] J. Chawla, S. Schardt, P. Lott, S. Angeli, S. Tischer, L. Maier, O. Deutschmann, *Chem. Eng. J.* **2024**, 148719. DOI: <https://doi.org/10.1016/j.cej.2024.148719>
- [32] K. A. Karinshak, P. Lott, M. P. Harold, O. Deutschmann, *ChemCatChem* **2020**, *12* (14), 3712–3720. DOI: <https://doi.org/10.1002/cctc.202000603>
- [33] S. Brunauer, P. H. Emmett, E. Teller, *J. Am. Chem. Soc.* **1938**, *60* (2), 309–319. DOI: <https://doi.org/10.1021/ja01269a023>
- [34] C. Karakaya, O. Deutschmann, *Appl. Catal., A* **2012**, *445–446*, 221–230. DOI: <https://doi.org/10.1016/j.apcata.2012.08.022>
- [35] D. Chan, S. Tischer, J. Heck, C. Diehm, O. Deutschmann, *Appl. Catal., B* **2014**, *156–157*, 153–165. DOI: <https://doi.org/10.1016/j.apcatb.2014.03.009>
- [36] S. Wan, K. Keller, P. Lott, A. B. Shirsath, S. Tischer, T. Häber, R. Suntz, O. Deutschmann, *Catal. Sci. Technol.* **2022**, *12* (14), 4456–4470. DOI: <https://doi.org/10.1039/D2CY00572G>
- [37] G. Bergeret, P. Gallezot, in *Handbook of Heterogeneous Catalysis* (Eds: G. Ertl, H. Knözinger, F. Schüth, J. Weitkamp), Wiley-VCH, Weinheim **2008**.
- [38] V. I. Savchenko, Y. S. Zimin, A. V. Nikitin, I. V. Sedov, V. S. Arutyunov, *Pet. Chem.* **2021**, *61* (7), 762–772. DOI: <https://doi.org/10.1134/S0965544121070021>
- [39] V. R. Choudhary, S. A. R. Mulla, V. H. Rane, *J. Chem. Technol. Biotechnol.* **1998**, *71* (2), 167–172. DOI: [https://doi.org/10.1002/\(SICI\)1097-4660\(199802\)71:2\(167:AID-JCTB789\)3.0.CO;2-F](https://doi.org/10.1002/(SICI)1097-4660(199802)71:2(167:AID-JCTB789)3.0.CO;2-F)
- [40] P. Ciambelli, L. Lisi, R. Pirone, G. Ruoppolo, G. Russo, *Catal. Today* **2000**, *61* (1–4), 317–323. DOI: [https://doi.org/10.1016/S0920-5861\(00\)00391-6](https://doi.org/10.1016/S0920-5861(00)00391-6)
- [41] X. Huang, D. Eggart, G. Qin, B. B. Sarma, A. Gaur, J. Yang, Y. Pan, M. Li, J. Hao, H. Yu, A. Zimina, X. Guo, J. Xiao, J.-D. Grunwaldt, X. Pan, X. Bao, *Nat. Commun.* **2023**, *14* (1), 5716. DOI: <https://doi.org/10.1038/s41467-023-41192-y>
- [42] D. Eggart, X. Huang, A. Zimina, J. Yang, Y. Pan, X. Pan, J.-D. Grunwaldt, *ACS Catal.* **2022**, *12* (7), 3897–3908. DOI: <https://doi.org/10.1021/acscatal.2c00092>
- [43] A. F. Holleman, E. Wiberg, N. Wiberg, *Lehrbuch der anorganischen Chemie*, 102nd ed., de Gruyter, Berlin **2007**.
- [44] P. Alphonse, B. Faure, *Microporous Mesoporous Mater.* **2014**, *196*, 191–198. DOI: <https://doi.org/10.1016/j.micromeso.2014.05.016>
- [45] B. Béguin, E. Garbowski, M. Primet, *Appl. Catal.* **1991**, *75* (1), 119–132. DOI: [https://doi.org/10.1016/S0166-9834\(00\)83128-0](https://doi.org/10.1016/S0166-9834(00)83128-0)
- [46] F. Oudet, P. Courtine, A. Vejux, *J. Catal.* **1988**, *114* (1), 112–120. DOI: [https://doi.org/10.1016/0021-9517\(88\)90013-9](https://doi.org/10.1016/0021-9517(88)90013-9)
- [47] T. Ren, L.-N. N. Nforbi, R. Kanakala, O. A. Graeve, *Inorg. Chem.* **2018**, *57* (6), 3035–3041. DOI: <https://doi.org/10.1021/acs.inorgchem.7b02635>
- [48] K. Patel, V. Blair, J. Douglas, Q. Dai, Y. Liu, S. Ren, R. Brennan, *Sci. Rep.* **2017**, *7*, 39946. DOI: <https://doi.org/10.1038/srep39946>
- [49] J. Heveling, *Ind. Eng. Chem. Res.* **2023**, *62* (6), 2353–2386. DOI: <https://doi.org/10.1021/acs.iecr.2c03007>
- [50] I. Tankov, K. Arishtirova, J. Bueno, S. Damyanova, *Appl. Catal., A* **2014**, *474*, 135–148. DOI: <https://doi.org/10.1016/j.apcata.2013.08.030>
- [51] K. O. Rocha, J. Santos, D. Meira, P. S. Pizani, C. Marques, D. Zanchet, J. Bueno, *Appl. Catal., A* **2012**, *431–432*, 79–87. DOI: <https://doi.org/10.1016/j.apcata.2012.04.022>
- [52] M. García-Diéguez, I. S. Pieta, M. C. Herrera, M. A. Larrubia, I. Malpartida, L. J. Alemany, *Catal. Today* **2010**, *149* (3–4), 380–387. DOI: <https://doi.org/10.1016/j.cattod.2009.07.099>
- [53] P. Malet, J. J. Benitez, M. J. Capitan, M. A. Centeno, I. Carrizosa, J. A. Odriozola, *Catal. Lett.* **1993**, *18* (1–2), 81–97. DOI: <https://doi.org/10.1007/BF00769501>
- [54] V. J. Ferreira, P. Tavares, J. L. Figueiredo, J. L. Faria, *Catal. Commun.* **2013**, *42*, 50–53. DOI: <https://doi.org/10.1016/j.catcom.2013.07.035>
- [55] S. Sarsani, D. H. West, W. Liang, V. Balakotaiah, *Chem. Eng. J.* **2017**, *328*, 484–496. DOI: <https://doi.org/10.1016/j.cej.2017.07.002>